PCCP

PAPER

View Article Online
View Journal

Cite this: DOI: 10.1039/c5cp06742a

Titanate cathodes with enhanced electrical properties achieved *via* growing surface Ni particles toward efficient carbon dioxide electrolysis

Lizhen Gan,[ab] Lingting Ye,*[a] Shanwen Tao[c] and Kui Xie*[a]

Received 5th November 2015,
Accepted 20th December 2015

DOI: 10.1039/c5cp06742a

www.rsc.org/pccp

Ionic conduction in perovskite oxide is commonly tailored by element doping in lattices to create charge carriers, while few studies have been focused on ionic conduction enhancement through tailoring microstructures. In this work, remarkable enhancement of ionic conduction in titanate has been achieved *via in situ* growing active nickel nanoparticles on an oxide surface by controlling the oxide material nonstoichiometry. The combined use of XRD, SEM, XPS and EDS indicates that the exsolution/dissolution of the nickel nanoparticles is completely reversible in redox cycles. With the synergetic effect of enhanced ionic conduction of titanate and the presence of catalytic active Ni nanocatalysts, significant improvement of electrocatalytic performances of the titanate cathode is demonstrated. A current density of 0.3 A cm^{-2} with a Faradic efficiency of 90% has been achieved for direct carbon dioxide electrolysis in a 2 mm-thick YSZ-supported solid oxide electrolyzer with the modified titanate cathode at 2 V and 1073 K.

Introduction

A solid oxide electrolyzer has huge potential to efficiently convert CO_2 into fuels with favourable kinetics and thermodynamics at high temperatures, which has been considered as an alternative to solve current energy and environmental crisis.[1] Conventional Ni/YSZ is being preferentially used as the composite cathode for high temperature carbon dioxide electrolysis in which the Ni cathode is always fed with a proportion of CO to avoid the oxidation of Ni to NiO.[2] As reported by Mogensen *et al.*, long term operation of CO/CO_2 electrolysis with Ni/YSZ is feasible,[3] the inherent redox instability of Ni/YSZ is an unsolved problem because the oxidation of Ni to NiO occurs if direct carbon dioxide electrolysis is conducted.[4] The Ni oxidation may lead to electrical conductivity loss, electrode performance degradation and even electrode delamination from the electrolyte.[3,5]

In contrast to Ni/YSZ, the perovskite titanate, $La_xSr_{1-x}TiO_{3+\delta}$ (LSTO), has been considered as the breakthrough in the field of solid oxide fuel cell anodes.[6] Reduced LSTO demonstrates typical metallic conductivity as high as 30–50 S cm^{-1} under reducing conditions even at high temperature.[7] As reported by Irvine *et al.*, direct steam electrolysis can be achieved using the LSTO cathode without reducing gas fed to the cathode and promising electrode polarizations are accordingly obtained.[8] In our previous work, we have also investigated direct CO_2 electrolysis with the composite cathode based on LSTO in an oxide-ion conducting solid oxide electrolyzer and found that the co-existence of CO_2 reduction and cathode reduction is competing to each other at high applied potential.[9] High applied potential facilitates the electrochemical reduction of LSTO and therefore enhances electronic conductivity of LSTO. However, the limitation of charge transfer is still present that restricts cathode activity, which is because of the limited ionic conduction of LSTO at high temperature.[9] On the other hand, the cathode activity is still limited by the insufficient activity of ceramic LSTO oxide in contrast to conventional Ni metal.

Ionic conduction enhancement is dependent on charge carrier concentrations while it is strongly dependent on the microstructure modified with metal particles as well. As reported by Tong *et al.*,[10] the ionic conductivity of $BaZr_{0.85}Y_{0.15}O_{3-\delta}$ has been increased by 1.5 times if Pd metal particles are dispersed on the ceramic surface. The presence of Pd in bulk has a negligible effect on ionic conductivity; however, significant enhancement can be achieved once the metal is exsolved on the surface. The grain and bulk conductivity can be together enhanced if

[a] *Key Lab of Design & Assembly of Functional Nanostructure, Fujian Institute of Research on the Structure of Matter, Chinese Academy of Sciences, Fuzhou, Fujian 350002, China. E-mail: ltye@fjirsm.ac.cn, kxie@fjirsm.ac.cn; Fax: +86-591-63179173; Tel: +86-591-63179173*

[b] *School of Mechanical and Automotive Engineering, Hefei University of Technology, No. 193 Tunxi Road, Hefei, Anhui 230009, China*

[c] *Department of Chemical Engineering, School of Engineering, University of Warwick, Coventry, CV4 7AL, UK*

metal is exsolved from bulk to the surface. As reported by Liu *et al.*, a fine microstructure with Ni and $BaZr_{0.1}Ce_{0.7}Y_{0.1}Yb_{0.1}O_{3-\delta}$ has led to a remarkable hydrogen permeation flux at 973–1173 K.[11] Because Ni not only offers fast electron conduction, but also enhances surface exchange kinetic and mechanical stability of the hydrogen separation membrane. For an active metal like Ni, the doped Ni is in the YSZ lattice while internal reduction would initially form Ni^0 along the YSZ grain boundaries as the growth of a reaction front from the surface to the interior, and it is beneficial for transporting charge carriers through the thickness of the reacted region. Then Ni^0 is *in situ* grown on the YSZ surface that is accordingly favorable for ionic conductivity enhancement.[12] According to the density functional theory (DFT) calculations, metallic particles like Pd and Ni catalysts favor ion transport especially on the metal–ceramic surface. And the energy cost associated with ion transfer reaction is strongly related to the nature of chemical contact at metal–ceramic interfaces.[13] On the other hand, the loading of metal catalysts is a common method to enhance cathode activity. For example, the impregnation of Ni on the LSTO cathode has demonstrated improved electrode polarization and accordingly increased the cathode kinetics and Faradic efficiency for direct steam electrolysis.[14] However, the agglomeration of metal nanoparticles is a big problem that degrades electrode performance if high temperature electrolysis is operated for a longer time.[15,16] An alternative method is to incorporate the metallic element as a dopant within a host lattice during the synthesis in air, which is then exsolved on the surface in the form of catalytically active metallic nanoparticles or micron-particles under reducing conditions. Upon re-oxidation, the dopant is re-incorporated into the host lattice, yielding a regenerative nanoparticle in the composite electrode.[17] The heterojunction interface between Ni nanoparticles and the oxide substrate is expected to prohibit the agglomeration of nanometal and therefore substantially enhances cathode stability activity.[18]

In this work, A-site deficient and B-site excess titanate, $(La_{0.3}Sr_{0.7})_{0.9}Ti_{0.95}Ni_{0.05}O_{3-\delta}$ (LSTNO), is designed to *in situ* grow Ni nanoparticles on the titanate surface. The presence of Ni nanoparticles is expected to both facilitate ion conduction in titanate and improve electrocatalytic activity. The electrical and electrochemical properties of the prepared cathode are systematically studied. Direct carbon dioxide electrolysis is then systematically investigated in the oxide-ion conducting solid oxide electrolyzers at 1073 K.

Experimental

All the chemicals (99.9%, AR) were purchased from SINOPHARM Chemical Reagent Co. Ltd (China). The powders of $(La_{0.3}Sr_{0.7})_{0.9}Ti_{0.95}Ni_{0.05}O_{3-\delta}$ (LSTNO) were synthesized by the high temperature solid state reaction method.[19] The powders of $(La_{0.8}Sr_{0.2})_{0.95}MnO_{3-\delta}$ (LSMO) were synthesized using solid state reaction by mixing the appropriate amounts of La_2O_3, $SrCO_3$ and MnO_2 and the treatment temperature was 1373 K (3 K min^{-1}) for 10 h in air.[20] The $Ce_{0.8}Sm_{0.2}O_{2-\delta}$ (SDC) powders were prepared by the combustion method in which the Sm_2O_3 and $Ce(NO_3)_3{\cdot}6H_2O$ powders were mixed evenly and sintered at 1073 K (3 K min^{-1}) for 3 h in air.[21] All the phase formations of LSTNO, LSTO, LSMO and SDC powders were analyzed using X-ray diffraction (XRD, 2θ = 3° min^{-1}, D/MAX2500V, Rigaku Corporation, Japan). In addition, X-Ray Photoelectron Spectroscopy (XPS) was performed on a Thermo ESCALAB 250 to analyze the surface of the oxidized and reduced LSTNO sample powders, and the binding energies were calibrated to the C1s peak at 284.6 eV.

Approximately 2.0 g of LSTNO and LSTO powders were pressed into disks under 6–8 MPa and then sintered at 1673 K for 10 h in air for the ionic conductivity test. The relative density of the sintered samples reached approximately 75–85%. The ionic conductivity of samples was tested *versus* temperature by the electron-blocking electrode method under oxidized and reduced conditions, respectively.[22,23] Before the ionic conductivity test of reduced samples, the disks of LSTNO and LSTO were reduced at 1673 K for 10 h in 5%H_2/Ar, respectively. The DC four-terminal method was used for reduced samples in the reducing atmosphere (5%H_2/Ar) and oxidized samples in the oxidizing atmosphere (air). The temperature was ranging from 673 to 1073 K with a step of 3 K min^{-1} while the conductivity was recorded using an online multi-meter (Keithley 2000, Digital Multimeter, Keithley Instruments Inc., USA) at a time step of 10 s. The conductivity was recorded *versus* temperature from 673 to 1073 K.

The YSZ electrolyte support with a thickness of 1 mm was made by dry-pressing the YSZ powders into a disk with a diameter of approximately 15 mm, followed by a sintering at 1823 K for 20 h in air. The two surfaces of the electrolyte were mechanically polished and ultrasonically washed in ethanol and distilled water. The slurries of cathode LSTNO/SDC or LSTO/SDC were prepared by milling LSTNO or LSTO powders with SDC powders at a weight ratio of 65 : 35 in alpha-terpineol with the appropriate amount of cellulose additive.[24] The LSMO and SDC powders were also mixed together at a weight ratio of 65 : 35 in alpha-terpineol with the appropriate amount of cellulose additive to prepare the anode slurry. Then, the two kinds of slurries were coated onto the two sides of the electrolyte in the area of approximately 1 cm^2 and the sample was sintered at 1273 K for 3 h in air. The current collector of silver paste (SS-8060, Xinluyi, Shanghai, China) was printed on both surfaces of the electrodes. The silver wire (0.2 mm in diameter) was used to form the circuit using conductive adhesives (DAD87, Shanghai Research Institute for Synthetic Resins, Shanghai, China), and treated at 823 K for 0.5 h in air. The symmetric cell was prepared in the above same way. The AC impedance spectroscopy for the different symmetric cells was studied at the open circuit voltage (OCV) under different H_2 and CO partial pressures at 1073 K using an Electrochemical Station (IM6, Zahner, Germany). The flow rates of the gases at 20 ml min^{-1} and different hydrogen and CO partial pressures were controlled using a mass flow meter (D08-3F, Sevenstar, Beijing, China). The electrolysis cells were sealed with a homemade testing jig using ceramic paste (JD-767, Jiudian, Dongguan, China) for the electrochemical test. The fuel electrode reduction was conducted by flowing 5%H_2/Ar at the flow rate of 50 mL min^{-1} for 1.5 h and then

pure hydrogen at the flow rate of 50 mL min^{-1} was supplied to the cathode for 2.0 h at operation temperature. After that the cathode would be sufficiently reduced and activated. Finally, the CO_2 electrolysis was performed. The CO_2 electrolysis in the solid oxide electrolyzer based on the LSTNO/SDC and LSTO/SDC cathode was tested under different applied voltages (from 1.2 to 2.0) at 1073 K in CO_2. The AC impedance spectra and the current density *versus* voltage curve (*I–V* curve) of the electrolysis cell were recorded. The online gas chromatograph (GC2014, Shimazu, Japan) was used to analyze the CO concentration of the output gas from the electrolyzer cells.

Results and discussion

Fig. 1(a1) and (b1) show the XRD Rietveld refinement patterns of the LSTO and LSTNO powders synthesized at 1073 K in air, respectively. Fig. 1(a2) and (b2) show the profiles of the LSTO and LSTNO powders after reduction, respectively. The experimental and calculated results indicated the perovskite structure with a space group of $Pm\bar{3}m$ for both oxidized and reduced samples.[25] The refinement of the oxidized and reduced LSTO samples gives the χ^2, wR_p and R_p values of 1.452, 7.47% and 5.67% and 1.467, 8.11% and 6.25%, respectively, indicating a close fit to the experimental data. The crystal cell parameter of the oxidized LSTO is 3.9069(27) Å which is slightly smaller than that of the reduced LSTO, 3.91052(7) Å. The chemical oxidation state of Ti is +4 with ionic radii of 0.605 Å, however, a part of Ti^{4+} has been transformed into Ti^{3+} (0.67 Å) in the reduced LSTO which may cause the cell parameter expansion. Nevertheless, no phase transition was observed in the LSTO even after the high-temperature treatment in a reducing atmosphere, firmly verifying the superior redox stability of LSTO ceramics. In Fig. 1(b1), XRD Rietveld refinement patterns of single-phase LSTNO reveal the successful partial replacement of Ti by Ni in the B-site, the refinement of the oxidized LSTNO gives χ^2, wR_p and R_p values of 1.037, 6.11% and 4.74%. The cell parameter is 3.9097(31) Å for the oxidized LSTNO larger than that of the oxidized LSTO sample, which is because of the larger ionic radii of Ni^{2+} (0.69 Å) in contrast to Ti^{4+}. It is also observed that, as shown in Fig. 1(b2), a peak ($2\theta = \sim 44.5^\circ$) corresponds to Ni indicating the successful exsolution of Ni nanoparticles from the A-site deficient and B-site excess LSTNO while the perovskite structure with a space group of $Pm\bar{3}m$ was retained, suggesting the excellent redox stability of the parent material even though the doped metal was exsolved from the lattice to anchor on the LSTO surface.

In order to further study different chemical states of the elements in redox cycles of the samples, XPS is performed to test the oxidized and reduced LSTNO as shown in Fig. 2. All XPS results were fitted using a Shirley-type background subtraction method, and the background functions for different XPS spectra were fitted using 80% Gaussian and 20% Lorenz. All information of the XPS peak comes from the database of Thermo Fisher Scientific. As shown in Fig. 2(a1) and (b1), the strong peaks of Ti^{4+} and Ni^{2+} are observed in the oxidized LSTNO, respectively. In contrast, part of Ti^{4+} is chemically reduced to Ti^{3+} by treating the LSTNO samples in the reducing atmosphere as confirmed by the signal of Ti^{3+} in Fig. 2(a2). Similar chemical state changes of the Ti element are also observed in the LSTO sample before and after reduction, as shown in Fig. 2(c1) and (c2). In addition, the XPS spectra of the Ni element are shown in Fig. 2(b2), in which Ni in the oxidation state of the LSTNO is in the form of Ni^{2+} while Ni^0 (2p1/2) is observed at 870.17 eV for the reduced sample. The results of XPS show that Ni^0 exists in the reduced sample, which firmly confirms the successful exsolution of the Ni nano-catalyst and is consistent with the XRD.

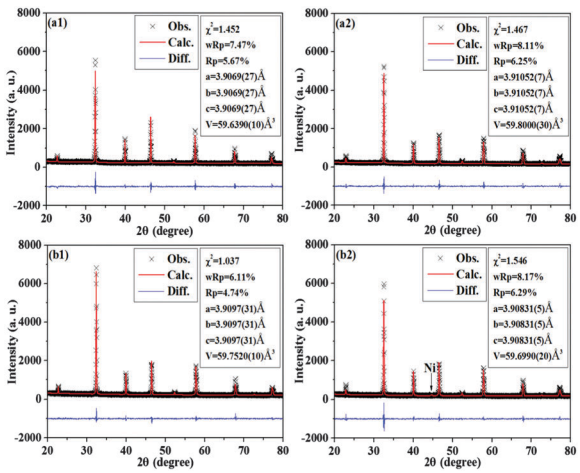

Fig. 1 XRD Rietveld refinement patterns of samples, (a1) oxidized LSTO; (a2) reduced LSTO; (b1) oxidized LSTNO; (b2) reduced LSTNO.

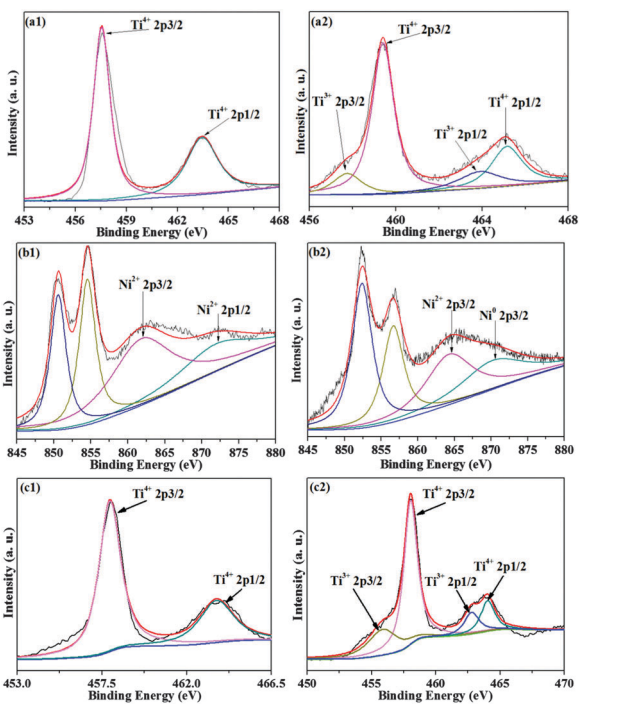

Fig. 2 XPS results of samples, (a1) Ti in oxidized LSTNO; (a2) Ti in reduced LSTNO; (b1) Ni in oxidized LSTNO; (b2) Ni in reduced LSTNO; (c1) Ti in oxidized LSTO; (c2) Ti in reduced LSTO.

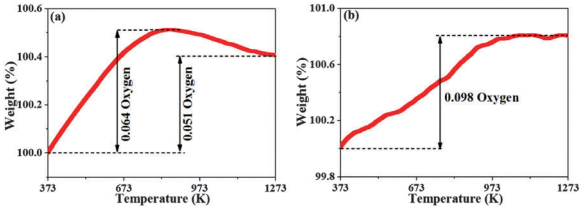

Fig. 3 TGA tests of the reduced LSTO (a) and the reduced LSTNO (b) from 373 to 1273 K in air.

In order to analyse the oxygen nonstoichiometry, TGA tests were performed for reduced LSTO and LSTNO from 373 to 1273 K (5 K min^{-1}) in air as shown in Fig. 3. The reduced LSTO demonstrated a chemical formula of $La_{0.3}Sr_{0.7}TiO_{3.086}$ accompanied by the 0.064 mol oxygen loss per chemical formula in contrast to the oxidized LSTO with a chemical formula of $La_{0.3}Sr_{0.7}TiO_{3.15}$ at 973 K. However, the change of Ti^{4+} to Ti^{3+} was not accompanied by the creation of the oxygen vacancy but the loss of excess interstitial oxygen. The chemical formula of the reduced LSTO was determined to be $La_{0.3}Sr_{0.7}TiO_{3.099}$ accompanied by the 0.051 mol oxygen loss per chemical formula. In contrast, the reduced LSTNO determined a chemical formula of $(La_{0.3}Sr_{0.7})_{0.9}Ti_{0.95}Ni_{0.05}O_{2.837}$ accompanied by the 0.098 mol oxygen loss per chemical formula. The weight increase (0.84 wt%) of LSTNO could be attributed to two processes: the oxidation of the reduced LSTO and the nickel nanoparticles. It is therefore estimated that almost all the nickel exsolved from the B-site after reduction in 5%H_2/Ar at 1073 K for 20 h. Moreover, SEM observation of the reduced LSTNO sample further confirms the exsolution of Ni nanoparticles anchoring on the surface of the reduced LSTNO as shown in Fig. 4(b). In comparison, the oxidized LSTNO is quite dense with a high level of sinter-ability exhibiting low level porosity as shown in Fig. 4(a).

Fig. 5(a) shows the temperature dependence of ionic conductivities of the oxidized LSTO and LSTNO in air from 673 to 1073 K,

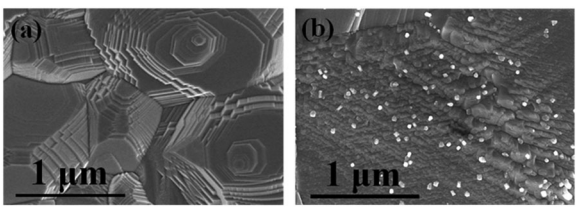

Fig. 4 SEM results of (a) oxidized LSTNO and (b) reduced LSTNO.

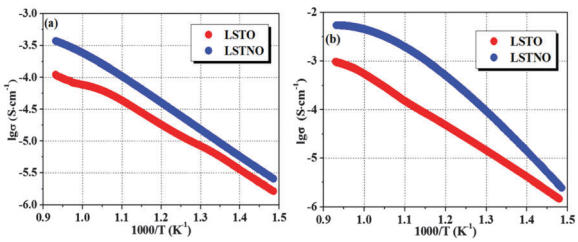

Fig. 5 The ionic conductivity of LSTO and LSTNO *versus* temperature from 673 to 1073 K, (a) oxidized conditions; (b) reduced conditions.

respectively. The ionic conductivity of the oxidized LSTNO improves with temperature and finally reaches 3.7 × 10^{-4} S cm^{-1} in air which is higher than the oxidized LSTO. This is because the doping of Ni in the lattice to create an oxygen vacancy is an effective method to increase the ionic conductivity.[26,27] In Fig. 5(b), the ionic conductivity of the reduced LSTNO reaches 5.4 × 10^{-3} S cm^{-1} with the reducing state at 1073 K. The introduction of nickel nanoparticles significantly enhances the ionic conductivity of LSTNO in contrast to the LSTO. Upon reduction, the LSTNO shows a high oxide ionic conductivity by ~1 order of magnitude higher than LSTO in a reducing atmosphere at 1073 K. The ionic conductivity is largely enhanced *via in situ* growing active nickel nanoparticles on the titanate surface. As reported, metallic nanoparticles like Pd and Ni catalyst favor ion transport especially on the metal–ceramic surface. And the energy cost associated with ion transfer reaction is strongly related to the nature of chemical contact at metal–ceramic interfaces.[13]

Fig. 6(a) and (b) present the microstructure of the YSZ electrolyte-supported half cells based on LSTO and LSTNO electrodes, respectively. The porous electrode layers are approximately 10 μm in thickness and the YSZ electrolyte supports were quite uniform and dense with the porous electrode layers adhered to the electrolyte very well. Fig. 7 was fitted using Zview software and shows the AC impedance of the symmetric cells based on the LSTO/SDC and LSTNO/SDC tested at 1073 K at different hydrogen partial pressures (pH_2). The ionic resistance of the YSZ electrolyte which mainly contributes to the resistances (R_s) is generally stable in a wide range of pH_2. In this case, all the series R_s have been set as 0 to compare the polarization resistances (R_p). As shown in Fig. 7(a), the R_p of the symmetric cell based on LSTO/SDC decreases from approximately 8.71 to 3.10 Ω cm^2 with the pH_2 ranging from 20% to 100%, suggesting that the stronger reducing atmosphere is beneficial for the improvement of the electrode polarizations. In contrast, the R_p of the symmetric cell based on LSTNO/SDC significantly improves from about 5.45 to 2.06 Ω cm^2 with increasing pH_2, which is probably due to the enhanced charge transfer and species diffusion in this composite electrode.

The direct electrolysis of pure CO_2 is researched in two kinds of solid oxide electrolyzers with cathodes based on LSTO/SDC and LSTNO/SDC under a series of applied voltages ranging from 1.0 to 2.0 V at 1073 K, respectively. In order to check the sealing of the single solid oxide electrolyzer based on the LSTO

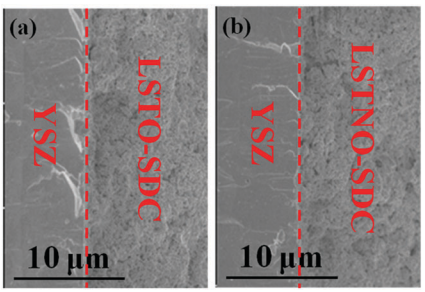

Fig. 6 Cross-sectional microstructure of the solid oxide symmetric and electrolyzer cells (a) LSTO–SDC and (b) LSTNO–SDC.

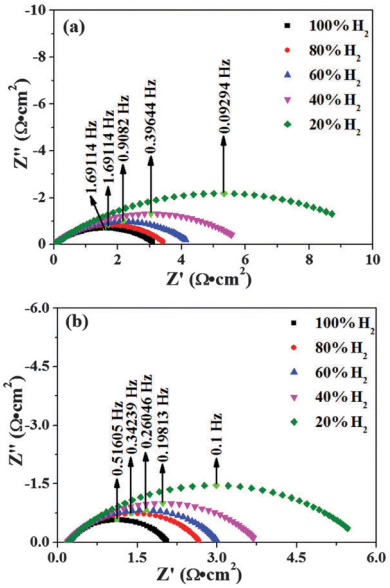

Fig. 7 The AC impedance of the symmetric cells for (a) LSTO and (b) LSTNO at different hydrogen partial pressures at 800 °C.

and LSTNO composite cathode, the open circuit voltage (OCV) is recorded with the cathode and anode exposed to 5%H_2/Ar and static air, respectively, to check the separation between the anodic and cathodic gases. The OCVs reach about 1.0 V for the cells, which indicates a good separation between the anodic and cathodic gas. Fig. 8(a) shows the typical curves of the current density *versus* voltage (*I–V* curves) of the electrolyzers for the direct carbon dioxide electrolysis. The maximum current density reaches about 240.1 mA cm^{-2} at 2.0 V based on the LSTO/SDC cathode at 1073 K while the current density based on the LSTNO/SDC cathode is greatly improved to approximately 318.1 mA cm^{-2} under the same conditions which is due to the presence of nickel catalysts anchored on the electrode surface. Above 1.0 V, the current densities of the LSTNO composite electrodes increase steeply compared with the LSTO composite cathode. In addition, the enhanced ionic conductivity of the LSTNO is also expected to improve the charge transfer in the electrode/YSZ interfaces. In order to study the electrolysis performance of the solid oxide electrolyzers with LSTO and LSTNO cathodes, cells are conducted with the composite cathodes fed pure CO_2 at 1073 K as shown in Fig. 8(b). Under the applied potential of 2.0 V, the current density of the solid oxide electrolyzer based on the LSTO composite cathode decreases from approximately 230 to 200 mA cm^{-2}, which is probably due to the local starvation of CO_2 at high voltage for the electrochemical reduction and the adsorption of CO_2 in the cathode as a limiting step. However, the current density with the LSTNO/SDC cathode is stable at high voltage and reaches 90.5, 137.1, 189.9, 248.9 and 316.8 mA cm^{-2} at 1.2 to 2.0 V, respectively; these values are much higher in contrast to the cell with the LSTO cathode under the same conditions, which indicate that the coupling between the metallic nickel and redox-stable titanate substrate with enhanced electrical properties has played a significant role in promoting the process of electrolysis reaction. Hence, the LSTNO composite cathode shows higher current density than LSTO at high voltages which can enhance the direct carbon dioxide electrolysis.

For further study of the change in R_s and R_p, as shown in Fig. 9, the *in situ* AC impedance spectroscopy is conducted under a series of applied voltages ranging from 1.0 to 2.0 V at 1073 K based on LSTO/SDC and LSTNO/SDC cathodes, respectively. It is observed that R_s values are generally stable, whereas R_p values obviously decrease as applied voltages increase from 1.0 to 2.0 V. It is assumed that increasing the voltage improves the electrode performances and R_p decreases remarkably. Increasing the voltage is expected to improve electrode polarization, following the improved kinetic process of the electrode. The applied voltage electrochemically reduces the composite cathode to enhance the mixed conductivity and therefore accordingly enhances the electrocatalytic activity of the composite electrode. Two semicircles are found from the impedance spectra: the high-frequency arcs (R_1) and low-frequency arcs (R_2). At high frequency, R_1 of the solid oxide electrolyzers with cathodes based on bare LSTO is decreased to approximately 0.48 Ω cm^2. In contrast, the R_1 for the cell with the LSTNO cathode is decreased to approximately 0.36 Ω cm^2 and is further enhanced under high applied potential. The R_1 is an indication of charge transfer at high frequency and the

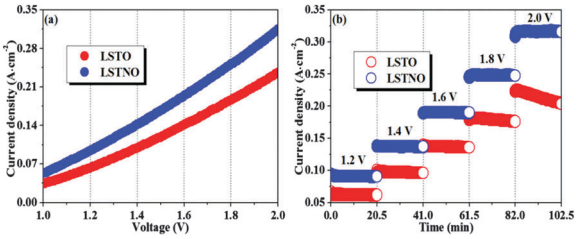

Fig. 8 (a) The *I–V* curves of two types of electrolyzers at 1073 K in CO_2; (b) the short-term performances of CO_2 electrolysis for the electrolyzer at 1073 K in CO_2.

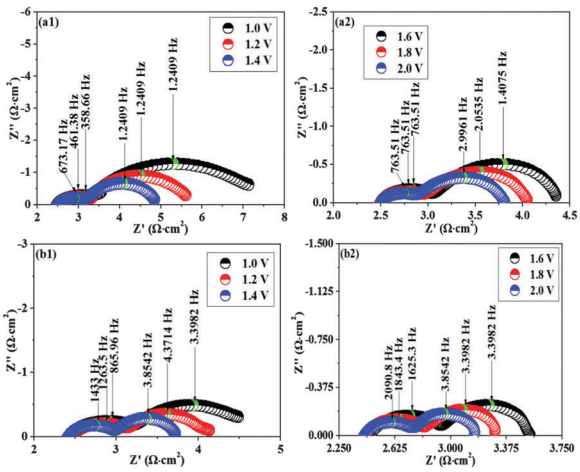

Fig. 9 The *in situ* AC impedance of the electrolysis cells based on (a1 and a2) LSTO and (b1 and b2) LSTNO at different voltages with the flow of CO_2 at 1073 K.

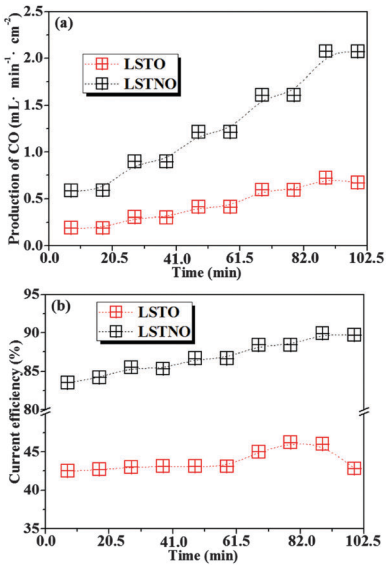

Fig. 10 The CO production (a) and current efficiency (b) for the electrolyzers with LSTO and LSTNO with the flow of CO_2 at 1073 K.

improved R_1 firmly indicates that the increased oxide-ion conductivity of LSTNO significantly benefits the charge transfer. At low frequency, it is observed that the mass transfer dominates the electrode process of the solid oxide electrolyzers, which is due to the dissociative adsorption, gas conversion and species transfer at the three-phase boundary. The R_2 for the cell based on the LSTO cathode remarkably improves from 4.41 to 0.93 Ω cm^2 with the applied voltage ranging from 1.0 to 2.0 V, suggesting the improved kinetics of gas conversion at high voltages. In contrast, the R_2 is based on the LSTNO cathode significantly reduced to 1.52 Ω cm^2 at low voltages and further enhanced to 0.44 Ω cm^2 at high voltages demonstrating the significantly improved mass transfer in the composite cathode. The results indicate that the synergetic effect of exsolved nickel nanoparticles and redox stable LSTO that leads to the largely improved electrical performances of the composite cathode in the solid oxide carbon dioxide electrolyzer.

Fig. 10 shows the rates of CO production and the current efficiencies of the electrolyzers with cathodes based on LSTO/SDC and LSTNO/SDC for CO_2 electrolysis at different applied voltages in pure CO_2. As shown in Fig. 10(a), the maximum CO production for the cell based on the LSTNO composite electrode was 2.074 mL min^{-1} cm^{-2}, which is much higher than 0.72 mL min^{-1} cm^{-2} at 2.0 V with the LSTO electrode. In addition, in Fig. 10(a), for the LSTO/SDC cathode, the maximum current efficiencies reach 46.39% in the flow of CO_2 at 1073 K. In contrast, the maximum current efficiency of the cell based on the LSTNO/SDC cathode was enhanced to 89.87% under the same conditions. The current efficiency is largely improved by about ~50% with LSTNO compared with bare LSTO at high voltage. Obviously, the solid oxide electrolyzer based on the LSTNO/SDC cathode exhibited better performances than the LSTO/SDC cathode. In order to validate the stability of the cathode, direct carbon dioxide electrolysis is performed at a fixed voltage of 1.5 V and 1073 K for 48 h with

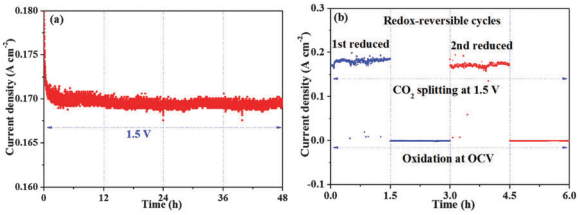

Fig. 11 (a) The performance of the LSTNO cathode with the flow of CO_2 at 1073 K; (b) the short-term performance of the LSTNO cathode after 2 redox cycles.

pure CO_2 fed in the cathode. As shown in Fig. 11(a), the current density with the LSTNO cathode is stabilized at 169.8 mA cm^{-2} even after an operation time of 48 h at high temperature, which confirms the excellent stability of the LSTNO cathode for direct carbon dioxide electrolysis. It should be noted that the cathode still demonstrates a comparable performance even after 2 redox cycles as shown in Fig. 11(b). The metallic Ni particles reversibly incorporate into the host lattice during the oxidation process in air and then reversibly exsolve on the titanate surface in the form of metallic catalyst nanoparticles under reducing conditions, yielding a regenerative composite electrode for high temperature carbon dioxide electrolysis.

Conclusions

Reversible exsolution of nickel nanoparticles anchored on the surface of LSTO through controlling nonstoichiometry of the A-site deficient and B-site doped titanate has been successfully achieved and utilized for the electrolysis of CO_2. The *in situ* growth of Ni nanoparticles on the LSTO surface has remarkably enhanced the ionic conductivity. The electrochemical properties of the composite electrodes in the symmetrical and electrolyzer cells were also systemically studied and the results show that the performances were significantly enhanced due to the presence of anchored catalytic-active nickel nanoparticles. The current efficiency of the electrolyzer based on the LSTNO/SDC cathode was enhanced by ~50% in contrast to the bare LSTO/SDC cathode for the electrolysis of CO_2. This study demonstrates that the presence of Ni nanoparticles is expected to both facilitate ion conduction in titanate and improve electrocatalytic activity for the electrolysis of CO_2.

Acknowledgements

This work was financially supported by the Natural Science Foundation of China (21303037 and 91545123) and the Ministry of Education of Overseas Returnees Fund (20131792).

References

1 K. R. Sridhar and B. T. Vaniman, *Solid State Ionics*, 1997, **93**, 321.
2 Q. X. Fu, C. Mabilat, M. Zahid, A. Brisse and L. Gautier, *Energy Environ. Sci.*, 2010, **3**, 1382.

3 S. D. Ebbesen and M. Mogensen, *J. Power Sources*, 2009, **193**, 349.
4 F. Bidrawn, G. Kim, G. Corre, J. T. S. Irvine, J. M. Vohs and R. J. Gorte, *Electrochem. Solid-State Lett.*, 2008, **11**, B167.
5 P. Kim-Lohsoontorn and J. Bae, *J. Power Sources*, 2011, **196**, 7161.
6 S. Li, Y. Li, Y. Gan, K. Xie and G. Meng, *J. Power Sources*, 2012, **218**, 244.
7 C. D. Savaniu and J. T. S. Irvine, *J. Mater. Chem.*, 2009, **19**, 8119.
8 K. Xie, Y. Zhang, G. Meng and J. T. S. Irvine, *Energy Environ. Sci.*, 2011, **4**, 2218.
9 Y. Li, J. Zhou, D. Dong, Y. Wang, J. Jiang, H. Xiang and K. Xie, *Phys. Chem. Chem. Phys.*, 2012, **14**, 15547.
10 J. Tong, A. Subramaniyan, H. Guthrey, D. Clark, B. P. Gorman and R. O'Hayre, *Solid State Ionics*, 2012, **211**, 26.
11 M. Liu, W. Sun, X. Li, S. Feng, D. Ding, D. Chen, M. Liu and H. C. Park, *Int. J. Hydrogen Energy*, 2013, **38**, 14743.
12 A. Subramaniyan, J. Tong, R. P. O'Hayre and N. M. Sammes, *J. Am. Ceram. Soc.*, 2011, **94**, 1800.
13 M. Malagoli, M. Liu, H. C. Park and A. Bongiorno, *Phys. Chem. Chem. Phys.*, 2013, **5**, 12525.
14 Y. Gan, Q. Qin, S. Chen, Y. Wang, D. Dong, K. Xie and Y. Wu, *J. Power Sources*, 2014, **245**, 245.
15 S. Xu, S. Chen, M. Li, K. Xie, Y. Wang and Y. Wu, *J. Power Sources*, 2013, **239**, 332.
16 P. Blennow, K. K. Hansen, L. R. Wallenberg and M. Mogensen, *Solid State Ionics*, 2009, **180**, 63.
17 D. Neagu, G. Tsekouras, D. N. Miller, H. Menard and J. T. S. Irvine, *Nat. Chem.*, 2013, **5**, 916.
18 H. Wei, K. Xie, J. Zhang, Y. Zhang, Y. Wang, Y. Qin, J. Cui, J. Yan and Y. Wu, *Sci. Rep.*, 2014, **4**, 5156.
19 S. Hashimoto, L. Kindermann, F. W. Poulsen and M. Mogensen, *J. Alloy Compd.*, 2005, **397**, 245.
20 H. He, Y. Huang, J. Regal, M. Boaro, J. M. Vohs and R. J. Gorte, *J. Am. Ceram. Soc.*, 2004, **87**, 331.
21 G. Jung and T. Huang, *J. Mater. Sci.*, 2003, **38**, 2461.
22 A. Endo, M. Ihara, H. Komiyama and K. Yamada, *Solid State Ionics*, 1996, **86**, 1191.
23 X. Li, H. Zhao, F. Gao, Z. Zhu, N. Chen and W. Shen, *Solid State Ionics*, 2008, **179**, 1588.
24 K. Xie, R. Yan, Y. Jiang, X. Liu and G. Meng, *J. Membr. Sci.*, 2008, **325**, 6.
25 A. D. Aljaberi and J. T. S. Irvine, *J. Mater. Chem. A*, 2013, **1**, 5868.
26 X. Li, H. Zhao, X. Zhou, N. Xu, Z. Xie and N. Chen, *Int. J. Hydrogen Energy*, 2010, **35**, 7913.
27 P. R. Slater, D. P. Fagg and J. T. S. Irvine, *J. Mater. Chem.*, 1997, **7**, 2495.